Electronic Supporting Information (ESI) for the manuscript entitled:

Bulky countercation effects on the crystal packing of anionic dithiooxalato-containing Ni(II), Pd(II) and Pt(II) complexes: spectroscopic-redox correlations

Nadia El Alouani Dahmouni, Anna Switlicka,* Barbara Machura, Nicolás Moliner, Renato Rabelo, Rafael Ruíz-García, Salah-Eddine Stiriba, Joan Cano and Miguel Julve*

Experimental section

Materials

Oxalyl chloride, benzenethiol, potassium hydrogen sulfide, tetraphenylarsonium chloride and benzyltriphenylphosphonium chloride were purchased from commercial sources and used as received. Potassium dithiooxalate and potassium bis(dithiooxalato-*k*²*S,S'*)metallate(II) (M = Ni, Pd and Pt) were prepared as previously described.[1,2]

Preparation of the compounds

Diphenyl dithiooxalate (Ph_2dto). Ph_2dto was prepared by following the procedure described in the literature[1] introducing some subtle modifications: oxalyl chloride (1.70 mL) was reacted with benzenethiol (4 mL) (1:2.6 molar ratio) in a round-bottom flask cooled with an ice bath and kept under continuous stirring. The flask was connected to a funnel which in turn was in contact with an aqueous solution of NaOH. The released HCl vapors during the reaction were so retained. The mixture took a yellowish colour and it gradually changed into a yellow crystalline solid. This solid was vaccum filtered and washed with small portions of absolute ethanol to remove the unreacted benzenethiol. Yield: 80%. X-ray suitable yellow needles of Ph_2dto were grown by recrystallization of the solid obtained in warm absolute ethanol. ^1H NMR (300 MHz, $CDCl_3$): δ = 7.45-7.55 (m, $H_{aromatics}$, 5H). ^{13}C NMR (75 MHz, $CDCl_3$): δ = 187 (C=O), 134.4, 130.2, 129.6, 125.5, 77.5 and 76.6 ($C_{aromatics}$). Selected IR data ν_{max}/cm^{-1}: 3098w, 3057m, 3021w, 3000w [ν(C-H)], 1797vs, 1678vs [ν_{as}(C=O)], 1582m [ν(C=C)], 1479s, 1440vs [ν_s(CO) + ν(CC) ring deformation], 1021s [?(CC) ring bending], 776vs, 739vs, 689s [ν(C-H) + ν(O=C-S)] and 614w [ν(C-S)].

$(BzPh_3P)_2[Ni(dto)_2]$ (1). A concentrated aqueous solution of $BzPh_3PCl$ (0.195 g, 0.5 mmol) was added to a warm aqueous solution of $K_2[Ni(dto)_2]$ (0.094 g, 0.25 mmol) under continuous stirring at room temperature. A dark purple solid immediately separated. After cooling the resulting suspension in an ice bath, the solid was separated by filtration, washed with cold water and air-dried. X-ray suitable dark violet elongated prisms of **1** were grown by recrystallization in dimethylformamide (dmf) at room temperature under air current in a hood. Yield: 95%. Anal. Calcd. for $C_{54}H_{44}NiO_4P_2S_4$ (**1**): C, 64.51; H, 4.38; S 12.76. Found: C, 64.02; H, 4.20; S, 12.62%. 1:4:2 Ni:S:P molar ratio. Selected IR data ν_{max}/cm^{-1}: 3080vw, 3058w, 2936w, 2898w, 2854vw [ν_s(C-H)], 1590vs, 1434s [ν(C=O)], 1494m [ν(C=C)], 1049s [ν(C-C) + ν(C-S)], 914m [ν_{as}(C-S) + ν(C-O)], 788m, 762w, 747m, 724m, 696s [ν(C-H)], 566vw [ν_s(C-S)].

$(BzPh_3P)_2[Pd(dto)_2]\cdot nCH_2Cl_2$ [n = 0 (2) and 3 ($2\cdot 3CH_2Cl_2$)]. A concentrated aqueous solution of $BzPh_3PCl$ (0.195 g, 0.5 mmol) was added to a warm aqueous solution of $K_2[Pd(dto)_2]$ (0.106 g, 0.25 mmol) under continuous stirring at room temperature. A pale yellow polycrystalline solid immediately appeared. After cooling the resulting suspension in an ice bath, the solid was separated by filtration, washed with cold water and air-dried. It was stored in an opaque container for ts protection from daylight. X-ray suitable large yellow prisms of **2** were grown by recrystallization of the bulk polycrystalline material in dmf at room temperature. Yield: 85%. Anal. Calcd. for $C_{54}H_{44}O_4P_2PdS_4$ (**2**): C, 61.58; H, 4.18; S, 12.18. Found: C, 61.07; H, 4.09; S, 12.07%. 1:4:2 Pd:S:P molar ratio. Selected IR data ν_{max}/cm^{-1} (**2**): 3082vw, 3058w, 2941w, 2901w, 2860vw [ν_s(C-H)], 1591vs, 1436s [ν(C=O)], 1494m [ν(C=C)], 1050s [ν(C-C) + ν(C-S)], 913m [ν_{as}(C-S) + ν(C-O)], 788m, 748s, 719m, 689s [ν(C-H)], 558vw [ν_s(C-S)].

Alternatively, the recrystallization in dichloromethane/diethyl ether mixtures after slow evaporation in a freezer afforded pale yellow needles of $\mathbf{2}\cdot 3CH_2Cl_2$. They loose crystallinity when removed from the mother liquor due to a relatively fast solvent loss to afford the non-solvated compound **2** (*vide infra*). The solvent contents of $\mathbf{2}\cdot 3CH_2Cl_2$ was determined by X-ray diffraction on single crystals which were embebed in paratone to preclude the solvent loss.

$(BzPh_3P)_2[Pt(dto)_2]$ (3). A concentrated aqueous solution of $BzPh_3PCl$ (0.195 g, 0.5 mmol) was added to a warm aqueous solution of $K_2[Pt(dto)_2]$ (0.128 g, 0.25 mmol) under continuous stirring at room temperature. An orange reddish polycrystalline solid was immediately separated. After cooling the resulting suspension in an ice bath, the solid was filtered, washed with cold water and air-dried. The recrystallization of the obtained solid in dmf at room temperature under air current in a fume hood afforded orange prisms of **3** which were suitable for X-ray diffraction. Anal. Calcd. for $C_{54}H_{44}O_4P_2PtS_4$ (**3**): C, 56.80; H, 3.86; S 11.23. Found: C, 56.48; H, 3.72; S, 11.03%. 1:4:2 Pt:S:P molar ratio. Selected IR data ν_{max}/cm^{-1}: 3094vw, 3058w, 2940w, 2901m, 2850vw [ν_s(C-H)], 1583vs, 1435s [ν(C=O)], 1494m [ν(C=C)], 1047s [ν(C-C) + ν(C-S)], 917m [ν_{as}(C-S) + ν(C-O)], 788m, 746s, 725m, 696s [ν(C-H)], 556w [ν_s(C-S)].

$(Ph_4As)_2[Ni(dto)_2]\cdot n(CH_3)_2CO$ with n = 0 (4) and 1 [$4\cdot(CH_3)_2CO$]. A concentrated aqueous solution of Ph_4ClAs (0.209 g, 0.5 mmol) was added to a warm aqueous solution of $K_2[Ni(dto)_2]$ (0.094 g, 0.25 mmol)

[1] H. O. Jones and H. S. Tasker, *J. Chem. Soc.*, 1909, **95**, 1904.

[2] E. G. Cox, W. Wardlaw and K. C. Webster, *J. Chem. Soc.,* 1935, 1475.

under continuous stirring at room temperature. A red polycrystalline solid was immediately separated. After cooling the resulting suspension in an ice bath, the solid was filtered, washed with cold water and air-dried. The recrystallization of the bulk polycrystalline solid in dmf at room temperature afforded **4** as dark red hexagonal prisms after standing in a hood for several days. Yield: 95%. Anal. Calcd. for $C_{52}H_{40}As_2NiO_4S_4$ (**4**): C, 58.61; H, 3.78; S 12.03. Found: C, 58.45; H, 3.95; S, 12.13%. 1:4:2 Ni:S:As molar ratio. Selected IR data ν_{max}/cm^{-1}: 3205w, 3152vw, 3085w, 3058m, 3024vw [ν_s(C-H)], 1601vs, 1439s [ν(C=O)], 1576m [ν(C=C)], 913m [ν_{as}(C-S) + ν(C-O)], 750s, 738m, 687s [ν(C-H)], 571w [ν_s(C-S)].

Alternatively, the recrystallization in an acetone/water mixture afforded dark red rhombuses of **4**·$(CH_3)_2CO$ after slow evaporation in a freezer, which were suitable for X-ray diffraction. Yield: 90%. Anal. Calcd. for $C_{55}H_{46}As_2NiO_5S_4$ [**4**·$(CH_3)_2CO$]: C, 58.79; H, 4.13; S 11.41. Found: C, 58.63; H, 4.12; S, 11.23%. 1:4:2 Ni:S:As molar ratio. Selected IR data ν_{max}/cm^{-1}: 3200w, 3154vw, 3075w, 3056m, 3020vw [ν_s(C-H)], 1713s [ν(C=O) from acetone], 1601vs, 1437s [ν(C=O)], 1575m [ν(C=C)], 916m [ν_{as}(C-S) + ν(C-O)], 744s, 688s [ν(C-H)], 565w [ν_s(C-S)].

$(Ph_4As)_2[Pd(dto)_2]$ (5). A concentrated aqueous solution of Ph_4AsCl (0.209 g, 0.5 mmol) was added to a warm aqueous solution of $K_2[Pd(dto)_2]$ (0.106 g, 0.25 mmol) under continuous stirring at room temperature. A pale yellow solid was immediately separated. After cooling the resulting suspension in an ice bath, the solid was filtered, washed with cold water and air-dried. The recrystallization of the bulk polycrystalline solid in dmf afforded yellow prims of **5** after slow evaporation in a freezer, as reported earlier.[3] Yield: 80%. Anal. Calcd. for $C_{52}H_{40}As_2O_4PdS_4$ (**5**): C, 56.11; H, 3.59; S 11.52. Found: C, 55.89; H, 3.48; S, 11.21%. 1:4:2 Pd:S:As molar ratio. Selected IR data ν_{max}/cm^{-1}: 3200w, 3150vw, 3085w, 3057m [ν_s(C-H)], 1602vs, 1437s [ν(C=O)], 1577m [ν(C=C)], 911m [ν_{as}(C-S) + ν(C-O)], 747s, 688s [ν(C-H)], 559w [ν_s(C-S)].

$(Ph_4As)_2[Pt(dto)_2]$ (6). A concentrated aqueous solution of Ph_4AsCl (0.209 g, 0.5 mmol) was added to a warm aqueous solution of $K_2[Pt(dto)_2]$ (0.128 g, 0.25 mmol) under continuous stirring at room temperature. An orange reddish solid was immediately separated. After cooling the resulting suspension in an ice bath, the solid was filtered, washed with cold water and air-dried. The recrystallization of the bulk polycrystalline solid in dmf at room temperature afforded **6** as orange hexagonal prims after standing several days in a hood. Yield: 85%. Anal. Calcd. for $C_{52}H_{40}As_2O_4PtS_4$ (**6**): C, 51.97; H, 3.33; S 10.67. Found: C, 51.56; H, 3.17; S, 10.45%. 1:4:2 Pt:S:As molar ratio. Selected IR data ν_{max}/cm^{-1}: 3200w, 3151vw, 3082w, 3058m [ν_s(C-H)], 1598vs, 1439s [ν(C=O)], 1576m [ν(C=C)], 914m [ν_{as}(C-S) + ν(C-O)], 749s, 738m, 687s [ν(C-H)], 561w [ν_s(C-S)].

Physical measurements

Elemental analyses (C, H, N and S) were conducted with a Flash Smart Eager 200 elemental analyzer. The IR spectra were performed on a Nicolet 5700 spectrometer in the range 4000-400 cm^{-1} as KBr pellets. UV/Vis spectra were recorded in acetonitrile solutions at room temperature on a Jasco UV/Vis/NIR V-670 spectrophotometer. The value of the M:S:P/As molar ratio (M = Ni, Pd and Pt) was determined by means of X-ray microanalysis with a Philips XL-30 scanning electron microscopy (SEM). A TA Instruments TGA550 thermobalance was used to determine the solvent contents in **2**·$3CH_2Cl_2$ and **4**·$(CH_3)_2CO$ under a 20 cm^3 min^{-1} flow rate of dinitrogen and the temperature being ramped from room r.t. to 600 °C (working speed of 100 °C min^{-1}).

Cyclic voltammetry was performed using an AUTOLAB 204 potentiostat/galvanostat. Cyclic voltammograms were carried out at room temperature using 0.1 M *n*-Bu_4NPF_6 as supporting electrolyte and 1.0 mM of the compounds **4**–**6** in acetonitrile. The auxiliary electrode was a glassy carbon rod that was polished with 1.0 μm diamond powder, sonicated, washed with absolute ethanol and acetone, and air-dried. The reference electrode was AgCl/Ag separated from the test solution by a salt bridge containing the solvent/supporting electrolyte, with a platinum disk (0.32 cm^2) as working electrode. All experiments were performed in standard electrochemical cells under argon atmosphere. The investigated scan rate and potential ranges were 25 to 250 mV s^{-1} and –2.0 to +2.0 V *vs.* AgCl/Ag, respectively. Ferrocene (Fc) was added as internal standard at the end of the measurements. The formal potentials were measured at a scan rate of 200 mV s^{-1} and they were referred to the Fc^+/Fc couple. The values of the measured formal potential and the anodic to cathodic peaks separation of ferrocene under the same conditions are $E(Fc^+/Fc)$ = +0.42 V *vs.* AgCl/Ag and $\Delta E_p(Fc^+/Fc)$ = 140 mV (CH_3CN, 0.1 M *n*-Bu_4NPF_6, 25 °C).

[3] P. Román. J. M. Gutiérrez.Zorrilla, A. Luque, J. I. Beitia, C. Guzmán-Miralles and M. Martínez-Ripoll, *Acta Crystallogr.*, 1991, **C47**, 48.

Crystal structure determination and refinement

Single crystals of dimensions 1.108 × 0.175 × 0.241 (Ph_2dto), 0.052 × 0.077 × 0.155 (**1**), 0.161 × 0.168 × 0.178 (**2**), 0.234 × 0.326 × 0.353 (**2**·3CH_2Cl_2), 0.027 × 0.049 × 0.054 (**3**), 0.114 × 0.312 × 0.420 (**4**), 0.088 × 0.226 × 0.456 [**4**·$(CH_3)_2CO$] and 0.027 × 0.049 × 0.054 mm^3 (**6**) were used for data collection on a Bruker D8 Venture diffractometer with PHOTON II detector and by using monochromatized Mo-Kα radiation (λ = 0.71073 Å). The single crystals of **2**·3CH_2Cl_2 and **4**·$(CH_3)_2CO$ were embedded in a silicon oil (paratone) to avoid the putative loss of the solvent molecules of crystallization when extracted from the mother liquor.
The structures of Ph_2dto, **1**–**4**, **2**·3CH_2Cl_2, **4**·$(CH_3)_2CO$ and **6** were solved by direct methods and subsequently completed by Fourier recycling using the SHELXTL[4] software packages and refined by the full-matrix least-square refinements based on F^2 with all observed reflections. All non-hydrogen atoms were refined anisotropically. Hydrogen atoms were placed at calculated positions, refined using idealized geometries (riding model), and assigned fixed isotropic displacement parameters, d(C-H) = 0.93 Å, U_{iso}(H) = 1.2U_{eq}(C) (for aromatic) and d(C-H) = 0.96 Å, U_{iso}(H) = 1.5U_{eq}(C) (for CH_2). Two possible refinements in the centrosymmetric $P\overline{1}$ space group were tested for **2**·3CH_2Cl_2. The CH_2Cl_2 lying about the inversion centre was refined without the chlorine atom disorder and with the chlorine atom disorder over two positions. The latter refinement with the chlorine atom disorder was finally chosen as it gives a little better refinement crystallographic indexes. Despite many attempts, however, it was not possible to achieve a satisfactory refinement in the centrosymmetric $P2_1/n$ space group proposed by PLATON programme for **4**·$(CH_3)_2CO$. Introduction of different models of disorder into the refinement (containing two or more domains), led to worsening of refinement parameters, with many non-positive atoms (data not shown). The most important crystallographic data and refinement conditions of Ph_2dto, **1**–**4**, **2**·3CH_2Cl_2, **4**·$(CH_3)_2CO$ and **6** are summarized in Tables S1–S3 whereas selected bond lengths and angles are listed in Tables S4-S11. CrystalMaker and Mercury 2.4 programs have been used for the visualization of the structures.[5,6] CCDC 2162595 (Ph_2dto), 2162588 (**1**), 2162593 (**2**), 2162587 (**2**·3CH_2Cl_2), 2162589 (**3**), 2162590 (**4**), 2162591 [**4**·$(CH_3)_2CO$] and 2162592 (**6**).

[4] G.M. Sheldrick, *Acta Crystallogr., Sect. C: Struct. Chem.,* 2015, **71**, 3.
[5] *CrystalMaker*, CrystalMaker Software, Bicester, England, 2015.
[6] C. F. Macrae, I. J. Bruno, J. A. Chisholm, P. R. Edfinfton, P. McCabe, E. Pidcock, L. Rodríguez–Monge, R. Taylor, J. van de Streek and P. A. Wood, *J. Appl. Crystallogr*., 2008, **41**, 466.

Table S1. Summary of crystallographic and structure refinement data for Ph_2dto

Formula	$C_{14}H_{10}O_2S_2$
Formula weight (g mol^{-1})	274.34
Crystal system	Orthorhombic
Space group	*Pca*2$_1$
a (Å)	11.3511(7)
b (Å)	14.5086(10)
c (Å)	7.8221(4)
V (Å^3)	1288.21(14)
Z	4
ρ_{calc} (g cm^{-3})	1.415
μ (mm^{-1})	0.402
Flack parameter	–0.05(2)
T (K)	120(2)
Reflect. collcd.	38261
Reflect. obs. [$I > 2\sigma(I)$]	2622
Data/restraints/parameters	2839/0/203
R_1[a] [$I > 2\sigma(I)$]	0.0263
wR_2[b] [$I > 2\sigma(I)$]	0.0544
Goodness-of-fit, *S*[c]	1.112

[a] $R_1 = \sum(|F_o| - |F_c|)/\sum|F_o|$. [b] $wR_2 = [\sum w(F_o^2 - F_c^2)^2/\sum w(F_o^2)^2]^{1/2}$. [c] $S = [\sum w(|F_o| - |F_c|)^2/(N_o - N_p)]^{1/2}$.

Table S2. Summary of crystallographic and structure refinement data for **1**–**3** and **2**·3CH_2Cl_2

	1	**2**	**3**	**2**·3CH_2Cl_2
Formula	$C_{54}H_{44}NiO_4P_2S_4$	$C_{54}H_{44}O_4P_2PdS_4$	$C_{54}H_{44}O_4P_2PtS_4$	$C_{57}H_{50}Cl_6O_4P_2PdS_4$
Formula weight (g mol^{-1})	1005.78	1053.47	1142.16	1308.25
Crystal system	Monoclinic	Monoclinic	Monoclinic	Triclinic
Space group	$P2_1/c$	$P2_1/c$	$P2_1/c$	$P\bar{1}$
a (Å)	8.8968(3)	8.887(4)	8.8748(3)	8.7497(5)
b (Å)	16.8278(7)	16.831(7)	16.8070(5)	10.1139(6)
c (Å)	15.9140(7)	15.724(9)	15.6789(5)	16.8551(10)
α (°)	90	90	90	81.465(2)
β (°)	96.543(2)	96.01(2)	96.1440(10)	75.796(2)
γ (°)	90	90	90	81.299(2)
V (Å^3)	2367.02(16)	2339.0(2)	2325.21(13)	1419.65(15)
Z	2	2	2	1
ρ_{calc} (g cm^{-3})	1.411	1.496	1.631	1.530
μ (mm^{-1})	0.701	0.691	3.314	0.859
T (K)	298(2)	150(2)	120(2)	120(2)
Reflect. collcd.	83325	45264	35558	78201
Reflect. obs. [$I > 2\sigma(I)$]	4652	5138	4413	11514
Data/restraints/parameters	5652/0/383	5990/0/384	5431/0/311	12550/0/349
R_1[a] [$I > 2\sigma(I)$]	0.0378	0.0300	0.0261	0.0322
wR_2[b] [$I > 2\sigma(I)$]	0.0869	0.0609	0.0435	0.0675
Goodness-of-fit, *S*[c]	1.046	1.114	1.037	1.056

[a] $R_1 = \sum(|F_o| - |F_c|)/\sum|F_o|$. [b] $wR_2 = [\sum w(F_o^2 - F_c^2)^2/\sum w(F_o^2)^2]^{1/2}$. [c] $S = [\sum w(|F_o| - |F_c|)^2/(N_o - N_p)]^{1/2}$.

Table S3. Summary of crystallographic and structure refinement data for **4**, **6** and **4**·$(CH_3)_2CO$

	4	**6**	**4**·$(CH_3)_2CO$
Formula	$C_{52}H_{40}As_2NiO_4S_4$	$C_{52}H_{40}As_2O_4PtS_4$	$C_{55}H_{46}As_2NiO_5S_4$
Formula weight (g mol^{-1})	1065.63	1202.01	1123.71
Crystal system	Triclinic	Triclinic	Monoclinic
Space group	$P\bar{1}$	$P\bar{1}$	$P2_1$
a (Å)	11.0025(9)	10.939(3)	10.4267(5)
b (Å)	13.2382(11)	13.206(3)	52.731(2)
c (Å)	18.4636(15)	18.371(5)	13.8477(6)
α (°)	69.239(3)	110.997(10)	90
β (°)	77.795(3)	89.980(11)	100.580(2)
γ (°)	73.530(3)	106.566(10)	90
V ($Å^3$)	2393.0(3)	2359.4(11)	7484.2(6)
Z	2	2	6
ρ_{calc} (g cm^{-3})	1.479	1.692	1.496
μ (mm^{-1})	1.997	4.588	1.921
T (K)	273(2)	150(2)	120(2)
Reflect. collcd.	93768	71968	327123
Reflect. obs. [$I > 2\sigma(I)$]	11372	7849	35674
Data/restraints/parameters	13646/0/568	8333/0/568	37087/25/1820
R_1[a] [$I > 2\sigma(I)$]	0.0261	0.0137	0.0322
wR_2[b] [$I > 2\sigma(I)$]	0.0673	0.0399	0.0694
Goodness-of-fit, S[c]	1.028	0.921	1.076

[a] $R_1 = \sum(|F_o| - |F_c|)/\sum|F_o|$. [b] $wR_2 = [\sum w(F_o^2 - F_c^2)^2/\sum w(F_o^2)^2]^{1/2}$. [c] $S = [\sum w(|F_o| - |F_c|)^2/(N_o - N_p)]^{1/2}$.

Table S4. Selected bond lengths (Å) and angles (deg) for **1***

Bond lengths		Bond angles	
Ni(1)–S(1)	2.1705(6)	S(1)– Ni(1)–S(1)^i	180.0
Ni (1)–S(1)^i	2.1705(6)	S(1)– Ni(1)–S(2)	92.02(2)
Ni (1)–S(2)	2.1666(6)	S(1)–Ni(1)–S(2)^i	87.98(2)
Ni(1)–S(2)^i	2.1666(6)	S(1)–Ni(1)–S(2)^i	87.98(2)
		S(1)^i–Ni(1)–S(2)^i	180.0
		S(2)–Ni(1)–S(2)^i	180.0

*Symmetry code: (i) = -*x*, 1 - *y*, *z*.

Table S5. Selected bond lengths (Å) and angles (deg) for **2***

Bond lengths		Bond angles	
Pd(1)–S(1)	2.2959(11)	S(1)–Pd(1)–S(1)	180.0
Pd(1)–S(1)^i	2.2959(11)	S(1)–Pd(1)–S(2)	89.60(2)
Pd(1)–S(2)	2.2892(11)	S(1)–Pd(1)–S(2)^i	90.40(2)
Pd(1)–S(2)^i	2.2891(11)	S(1)^i–Pd(1)–S(2)	90.40(2)
		S(1)^i–Pd(1)–S(2)^i	89.60(2)
		S(2)–Pd(1)–S(2)^i	180.0

*Symmetry code: (i) = –*x*, 1 – *y*, –*z*.

Table S6. Selected bond lengths (Å) and angles (deg) for **2**·3CH_2Cl_2

Bond lengths		Bond angles	
Pd(1)–S(1)	2.2955(3)	S(1)–Pd(1)–S(1)^{ii}	90.184(9)
Pd(1)–S(1)^{ii}	2.2955(3)	S(1)–Pd(1)–S(2)	89.816(9)
Pd(1)–S(2)	2.3022(3)	S(1)–Pd(1)–S(2)^{ii}	180.0
Pd(1)–S(2)^{ii}	2.3022(3)	S(1a)–Pd(1)–S(2)	180.0
		S(1a)–Pd(1)–S(2)^{ii}	90.184(10)
		S(2)–Pd(1)–S(2)^{ii}	89.816(10)

*Symmetry code: (ii) = 1 – *x*, 1 – *y*, –*z*.

Table S7. Selected bond lengths (Å) and angles (deg) for **3***

Bond lengths		Bond angles	
Pt(1)–S(1)	2.2942(7)	S(1)–Pt(1)–S(1)^{i}	180.0
Pt(1)–S(1)^{i}	2.2942(7)	S(1)–Pt(1)–S(2)	89.62(2)
Pt(1)–S(2)	2.2901(7)	S(1)^{i}–Pt(1)–S(2)	90.38(2)
Pt(1)–S(2)^{i}	2.2902(7)	S(1)–Pt(1)–S(2)^{i}	90.37(2)
		S(1)^{i}–Pt(1)–S(2)^{i}	89.63(2)
		S(2)–Pt(1)–S(2)^{i}	180.0

*Symmetry code: (i) = -*x*, 1 - *y*, -*z*.

Table S8. Selected bond lengths (Å) and angles (deg) for **4**

Bond lengths		Bond angles	
Ni(1)–S(1)	2.1762(5)	S(1)–Ni(1)–S(2)	91.609(19)
Ni(1)–S(2)	2.1717(5)	S(1)–Ni(1)–S(3)	88.98(2)
Ni(1)–S(3)	2.1737(5)	S(1)–Ni(1)–S(4)	175.96(2)
Ni(1)–S(4)	2.1701(5)	S(2)–Ni(1)–S(3)	179.28(2)
		S(2)–Ni(1)–S(4)	87.48(2)
		S(3)–Ni(1)–S(4)	91.97(2)

Table S9. Selected bond lengths (Å) and angles (deg) for **4**·$(CH_3)_2CO$

Bond lengths		Bond angles	
Ni(1)–S(1)	2.1754(11)	S(1)–Ni(1)–S(2)	92.42(4)
Ni(1)–S(2)	2.1784(12)	S(1)–Ni(1)–S(3)	87.01(4)
Ni(1)–S(3)	2.1730(12)	S(1)–Ni(1)–S(4)	179.18(5)
Ni(1)–S(4)	2.1778(12)	S(2)–Ni(1)–S(3)	179.19(5)
		S(2)–Ni(1)–S(4)	88.33(5)
		S(3)–Ni(1)–S(4)	92.25(5)
Ni(2)–S(5)	2.1731(12)	S(5)–Ni(1)–S(6)	92.13(4)
Ni(2)–S(6)	2.1712(12)	S(5)–Ni(1)–S(7)	87.45(4)
Ni(2)–S(7)	2.1668(12)	S(5)–Ni(1)–S(8)	179.46(5)
Ni(2)–S(8)	2.1784(11)	S(6)–Ni(1)–S(7)	179.44(6)
		S(6)–Ni(1)–S(8)	88.08(4)
		S(7)–Ni(1)–S(8)	92.35(5)
Ni(3)–S(9)	2.1831(12)	S(9)–Ni(1)–S(10)	91.87(5)
Ni(3)–S(10)	2.1820(12)	S(9)–Ni(1)–S(11)	88.29(4)
Ni(3)–S(11)	2.1829(12)	S(9)–Ni(1)–S(12)	179.22(6)
Ni(3)–S(12)	2.1784(12)	S(10)–Ni(1)–S(11)	179.57(6)
		S(10)–Ni(1)–S(12)	87.74(5)
		S(11)–Ni(1)–S(12)	92.11(4)

Table S10. Selected bond lengths (Å) and angles (deg) for **5***

Bond lengths		Bond angles	
Pd(1)–S(1)	2.298(3)	S(1)–Pd(1)–S(2)	89.53(8)
Pd(1)–S(2)	2.302(3)	S(1)– Pd(1)–S(3)	176.10(8)
Pd(1)–S(3)	2.302(3)	S(1)– Pd(1)–S(4)	89.71(8)
Pd(1)–S(4)	2.298(3)	S(2)–Pd(1)–S(3)	91.61(8)
		S(2)–Pd(1)–S(4)	179.22(8)
		S(3)–Pd(1)–S(4)	89.14(8)

*Values taken from P. Román. J. M. Gutiérrez-Zorrilla, A. Luque, J. I. Beitia, C. Guzmán-Miralles and M. Martínez-Ripoll, *Acta Crystallogr.*, 1991, **C47**, 48.

Table S11. Selected bond lengths (Å) and angles (deg) for **6**

Bond lengths		Bond angles	
Pt(1)–S(1)	2.2967(8)	S(1)–Pt(1)–S(2)	89.06(2)
Pt(1)–S(2)	2.3007(7)	S(1)– Pt(1)–S(3)	89.87(2)
Pt(1)–S(3)	2.2939(7)	S(1)– Pt(1)–S(4)	179.276(18)
Pt(1)–S(4)	2.2997(8)	S(2)–Pt(1)–S(3)	176.184(19)
		S(2)–Pt(1)–S(4)	91.49(2)
		S(3)–Pt(1)–S(4)	89.55(2)

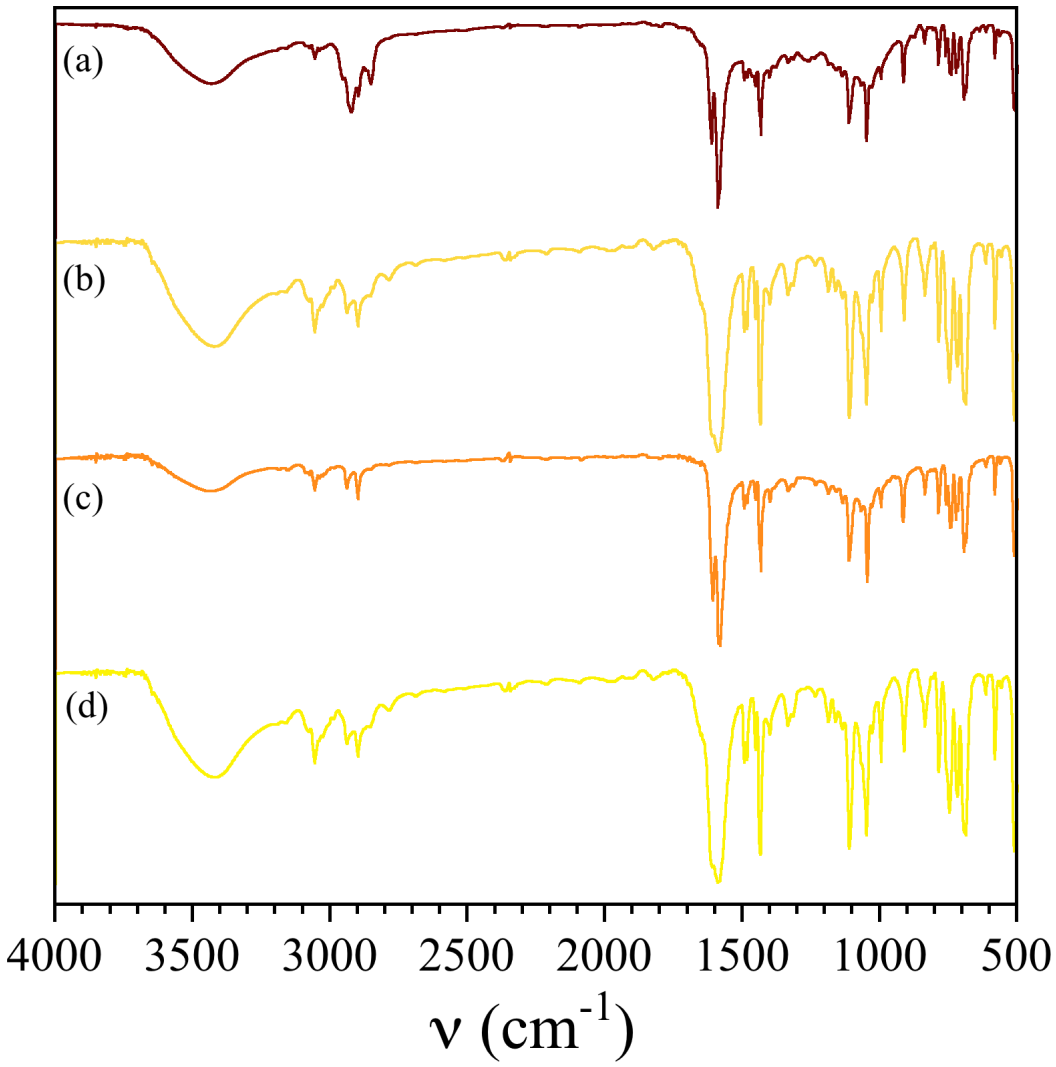

Fig. S1 IR spectra of **1** (a), **2** (b), **3** (c) and **2**·3CH_2Cl_2 (d) as KBr pellets.

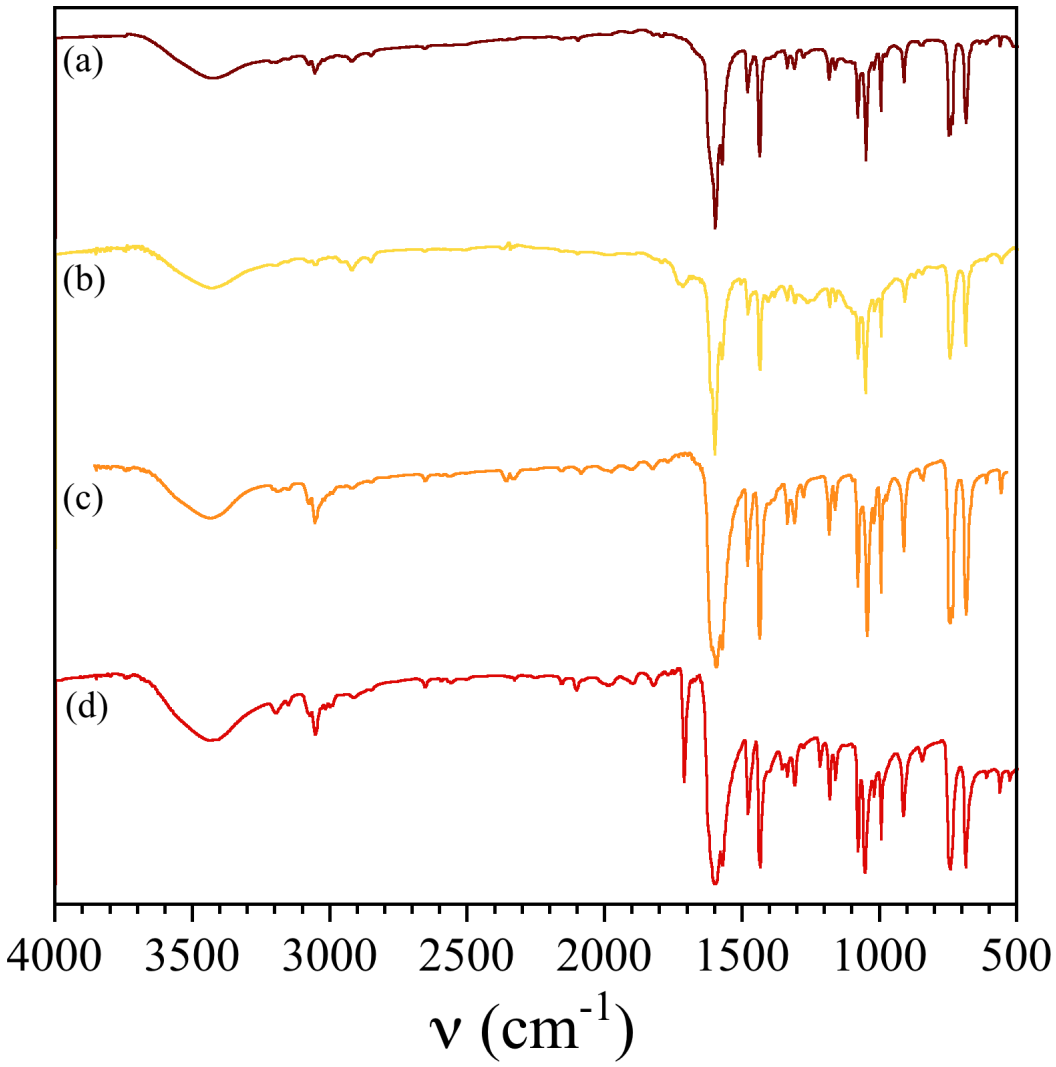

Fig. S2 IR spectra of **4** (a), **5** (b), **6** (c) and **4**·$(CH_3)_2CO$ (d) as KBr pellets.

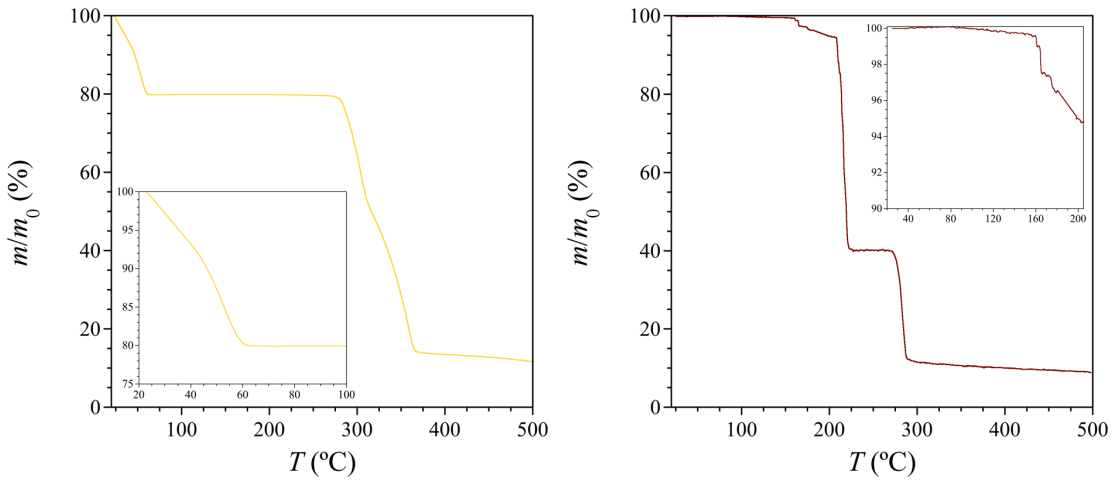

Fig. S3 TGA profile of **2**·3CH_2Cl_2 (a) and **4**·$(CH_3)_2CO$ (b) under a dry N_2 atmosphere. The inset shows an amplification of the desolvation process.

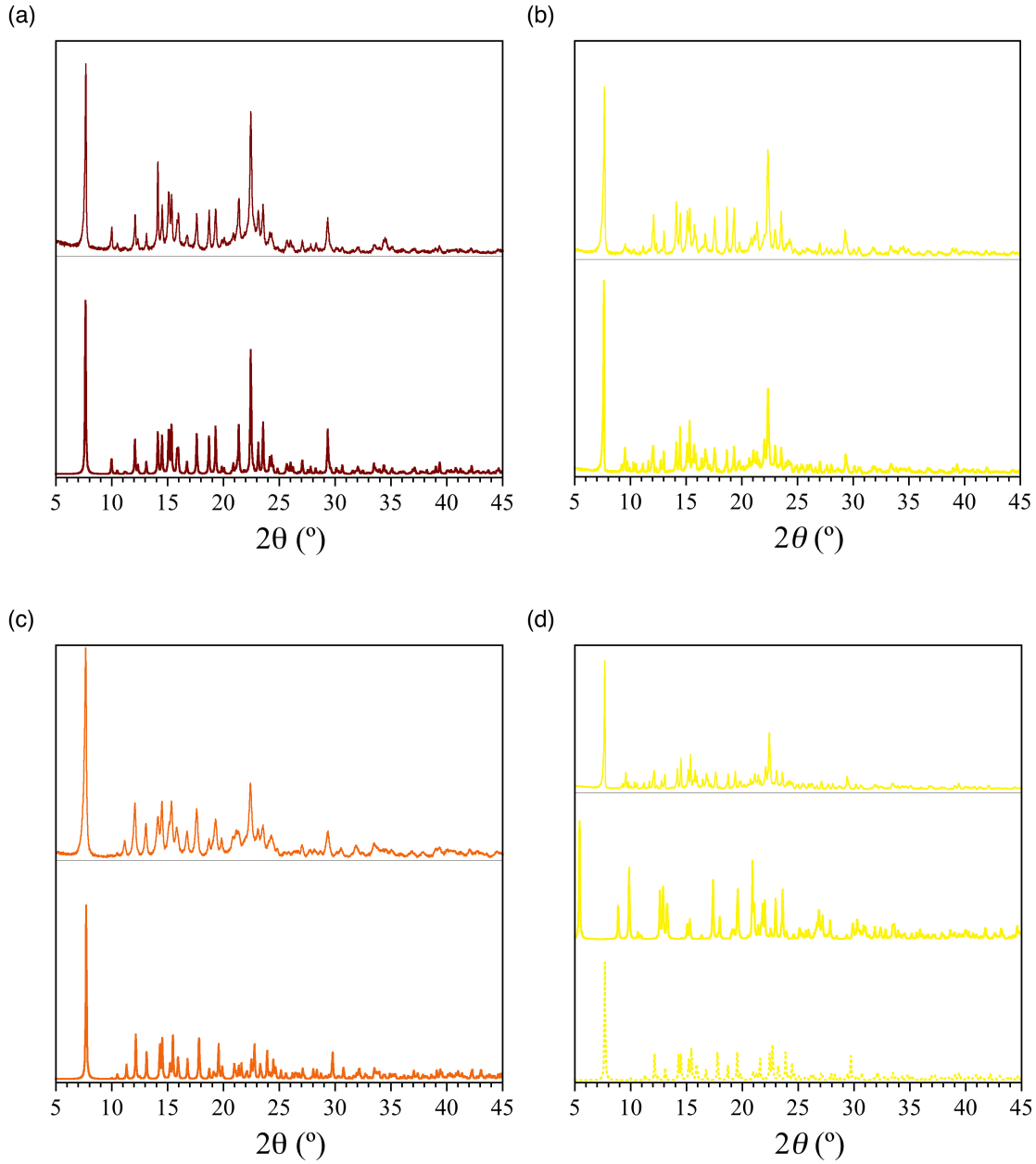

Fig. S4 Powder XRD patterns of **1** (a), **2** (b), **3** (c) and **2**·3CH_2Cl_2 (d) compared to the calculated ones (thicker lines). The yellow dotted line corresponds to the calculated XRD pattern of the desolvated derivative **2**.

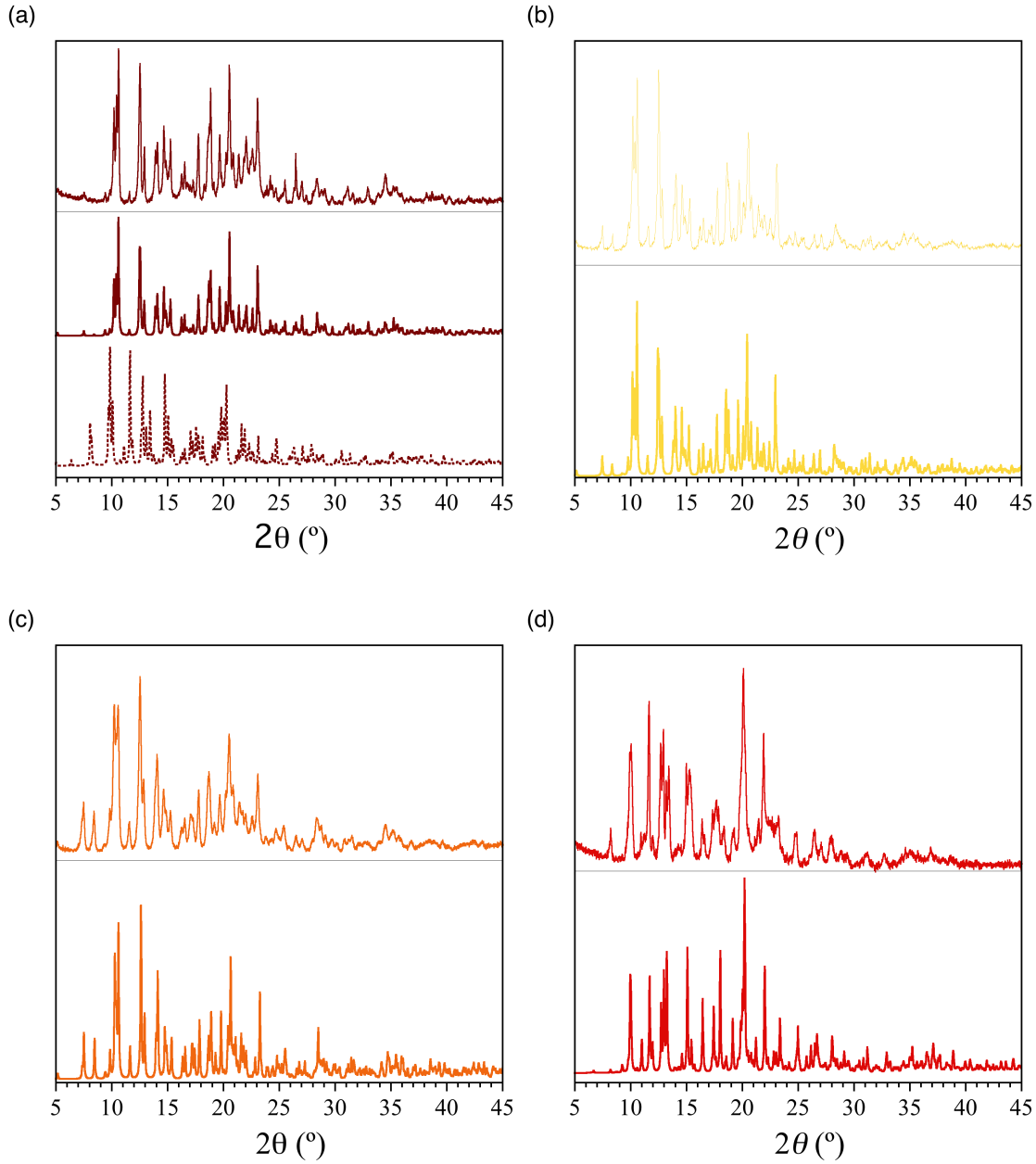

Fig. S5 Powder XRD patterns of **4** (a), **5** (b), **6** (c) and **4**·$(CH_3)_2CO$ (d) compared to the calculated ones (thicker lines). The purple dotted line corresponds to the calculated XRD pattern of polymorph **4'**.

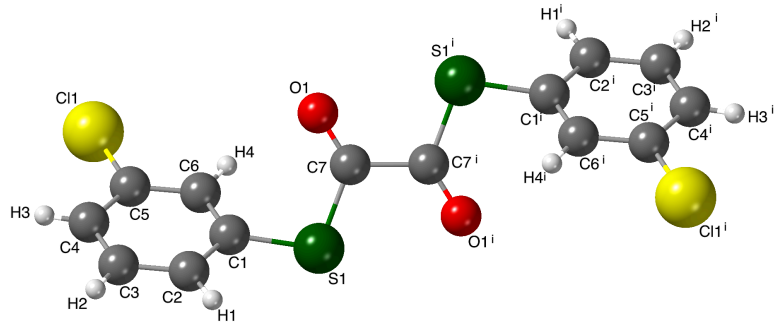

Fig. S6 The molecular structure of 3-ClPh$_2$dto with the atom numbering scheme [symmetry code: (i) = – *x*, 1 – *y*, 1 – *z*].

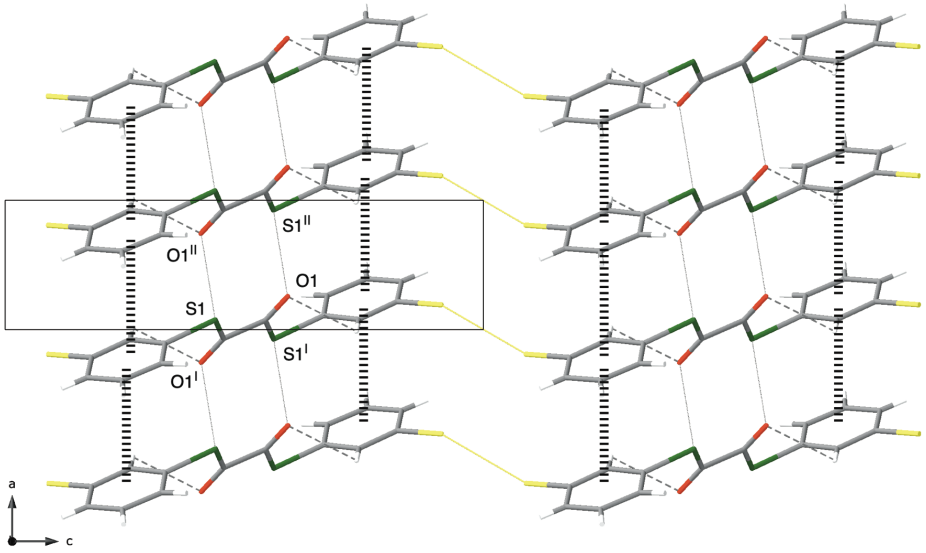

(a)

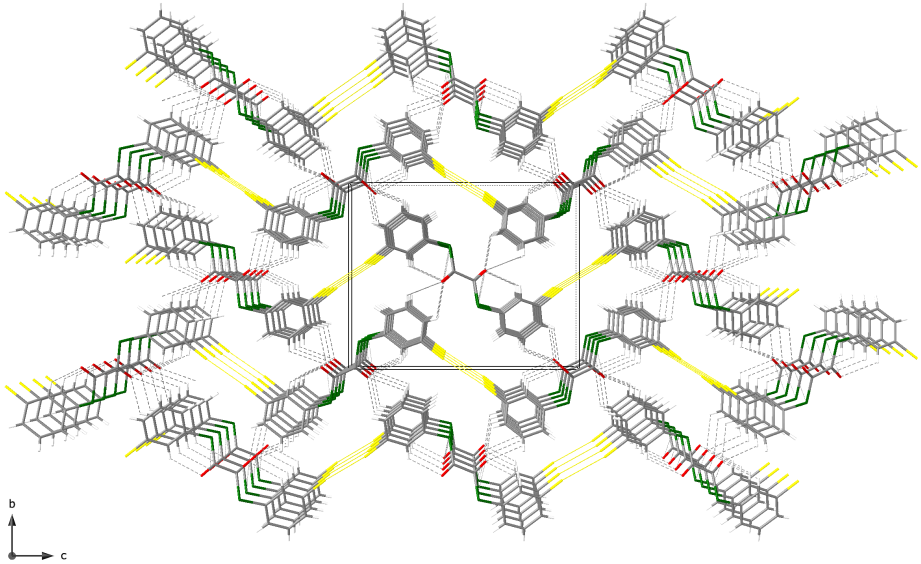

(b)

Fig. S7 (a) View of a fragment of the chalcogen-bridged ribbon-like chain of the neutral 3-ClPh$_2$dto molecules along the crystallographic *b* axis with the atom numbering scheme [symmetry code: (i) = – *x*, 1 – *y*, 1 – *z*; (ii) = 1 – *x*, 1 – *y*, 1 – *z*]. (b) Perspective view of the crystal packing of the neutral 3-ClPh$_2$dto molecules along the crystallographic *a* axis. The weak intermolecular C=O···S, C=O···H–C and C–H···π type interactions are represented by dotted, dashed and hashed lines, respectively.

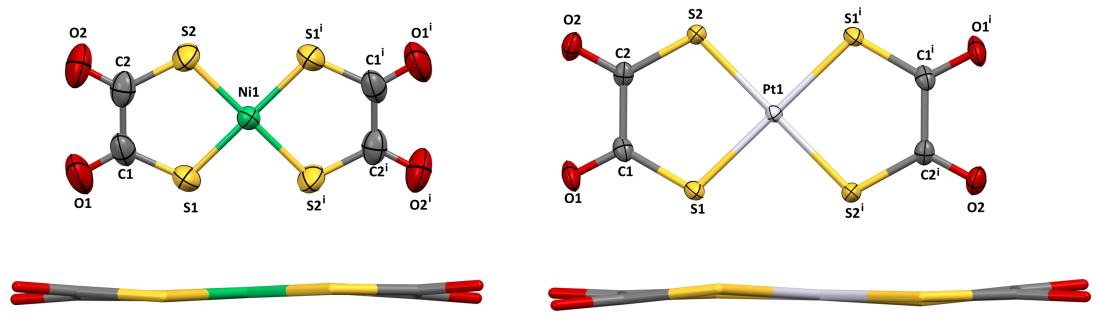

(a) (b)

Fig. S8 Front (top) and side (bottom) views of the $[M(dto)]^{2-}$ complex anions (M = Ni and Pt) of **1** (a) and **3** (b) together with the atom numbering [symmetry code: (i) = *–x*, 1 *–y*, *–z*].

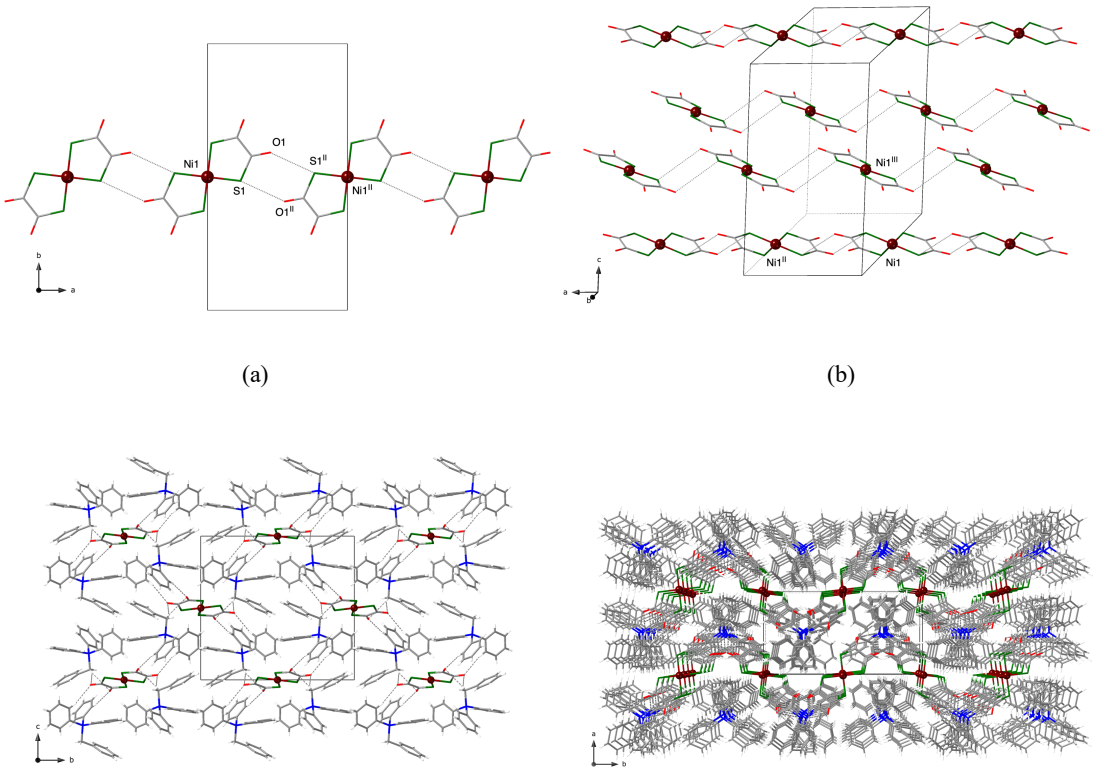

Fig. S9 Views of a fragment of the chalcogen-bridged chain (a) and the adjacent supramolecular zigzag chains (b) of the $[Ni(dto)]^{2-}$ complex anions of **1** together with the atom numbering [symmetry code: (ii) = 1 – *x*, 1 – *y*, –*z*; (iii) = – *x*, 1/2 + *y*, 1 – *z*]. Perspective views of the crystal packing of the $[Ni(dto)]^{2-}$ complex anions and $BzPh_3P^+$ countercations of **1** along the crystallographic *a* (c) and *c* (d) axes. The intermolecular C=O···S and C=O···H–C type interactions are represented by dotted and dashed lines, respectively.

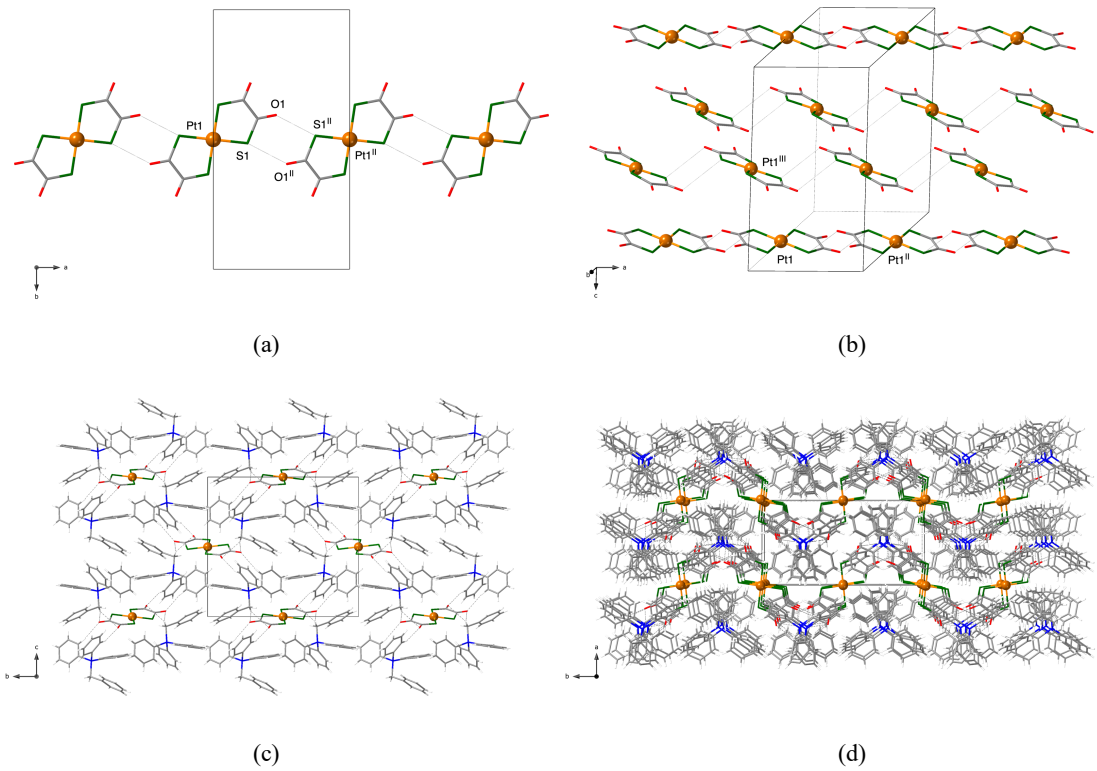

Fig. S10 Views of a fragment of the chalcogen-bridged chain (a) and the adjacent supramolecular zigzag chains (b) of the $[Pt(dto)]^{2-}$ complex anions of **3** together with the atom numbering [symmetry code: (ii) = 1 –*x*, 1 –*y*, –*z*; (iii) = –*x*, 1/2 + *y*, 1 – *z*]. Perspective views of the crystal packing of the $[Pt(dto)]^{2-}$ complex anions and $BzPh_3P^+$ countercations of **3** along the crystallographic *a* (c) and *c* (d) axes. The intermolecular C=O···S and C=O···H–C type interactions are represented by dotted and dashed lines, respectively.

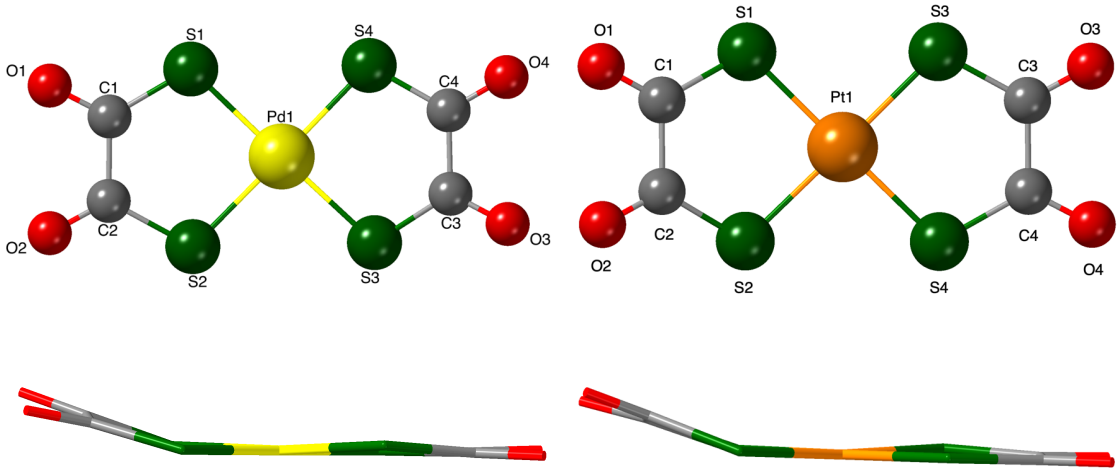

(a) (b)

Fig. S11 Front (top) and side (bottom) views of the $[M(dto)]^{2-}$ units (M = Pd and Pt) of **5** (a) and **6** (b) together with the atom numbering.

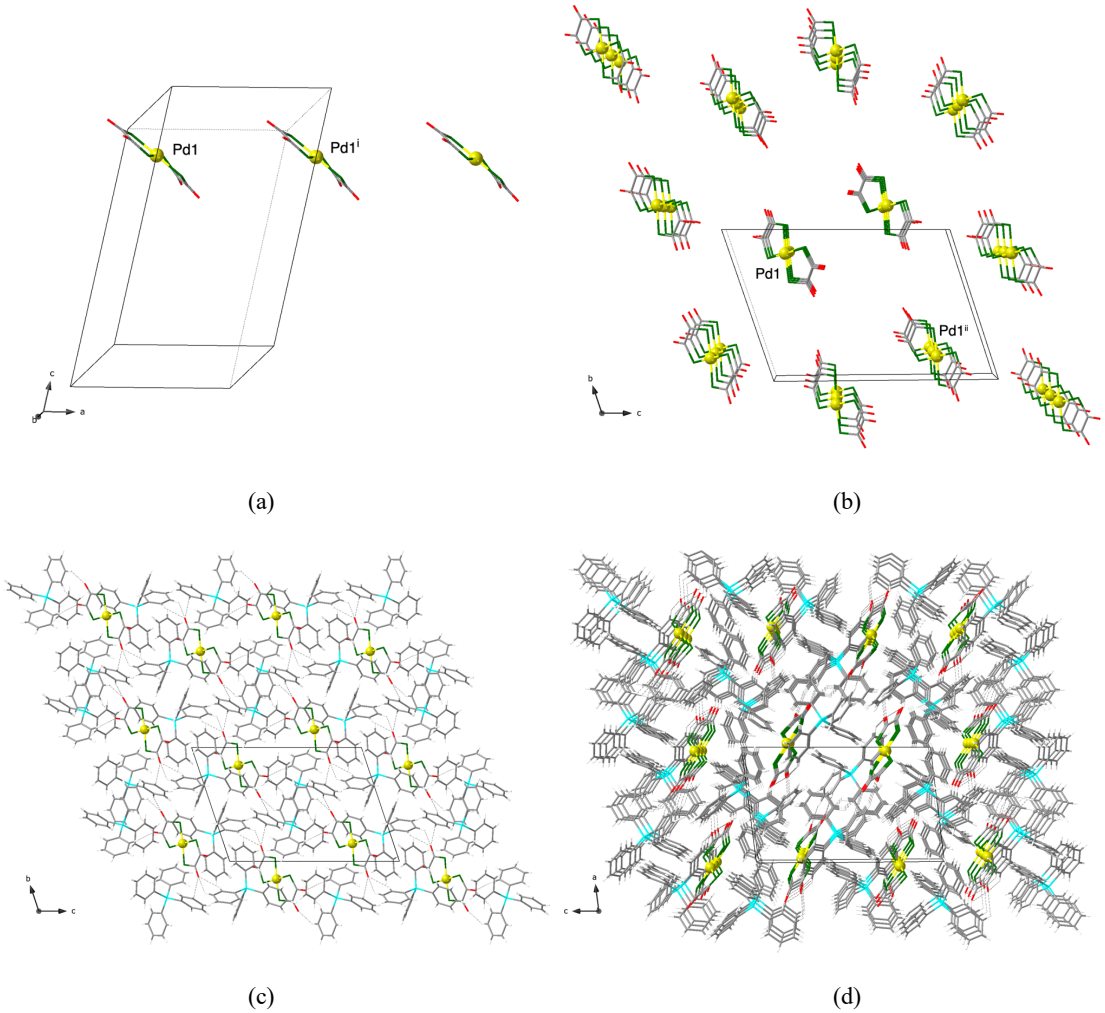

Fig. S12 Views of a linear (a) and the adjacent parallel linear (b) arrays of discrete $[Pd(dto)]^{2-}$ complex anions of **5** together with the atom numbering [symmetry code: (i) = 1 + *x*, *y*, *z*; (ii) = 1 – *x*, 1 – *y*, 1 – *z*]. Perspective views of the crystal packing of the $[Pd(dto)]^{2-}$ complex anions and Ph_4As^+ countercations along the crystallographic *a* (c) and *b* (d) axes, showing the segregated arrays of cations and anions in the crystallographic *bc* and *ac* planes, respectively. The intermolecular C=O···H–C type interactions are represented by dashed lines.

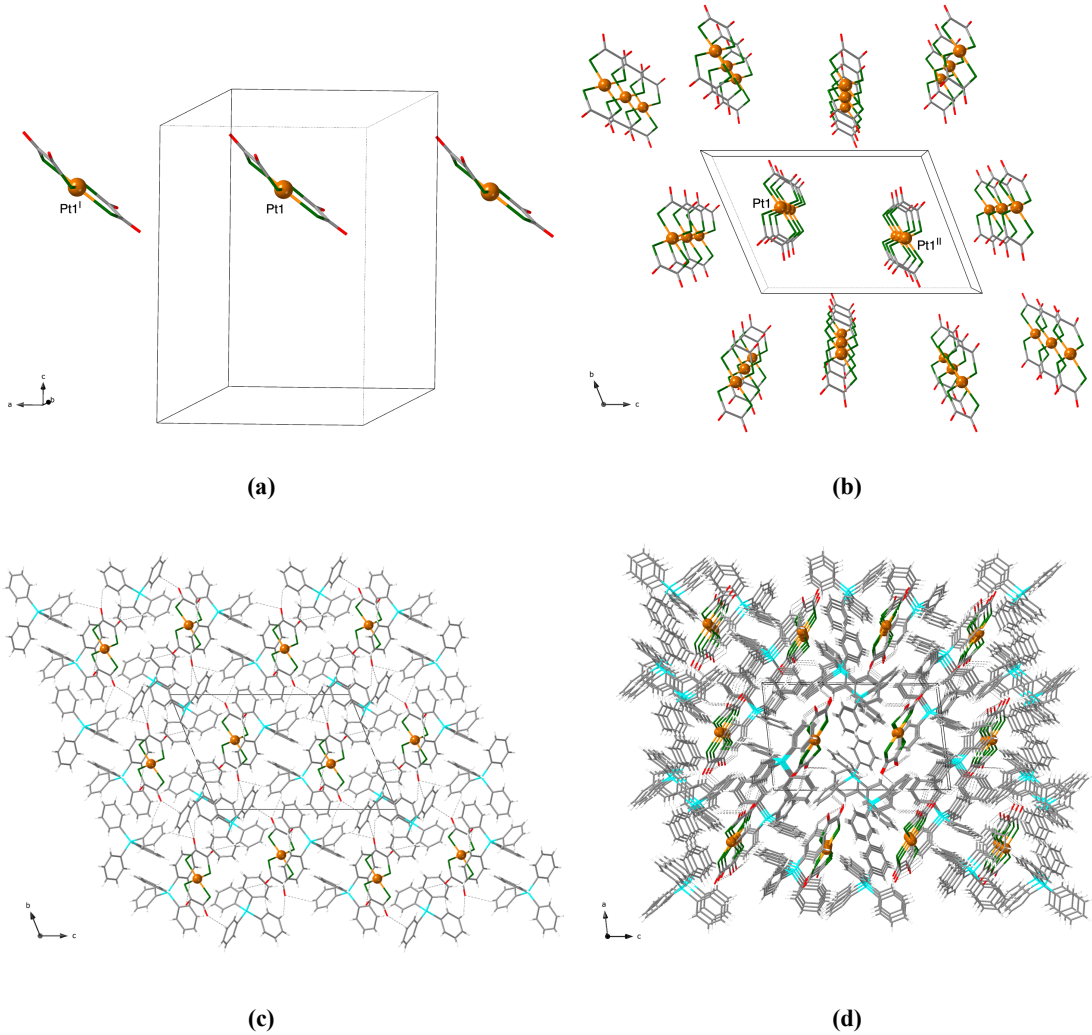

Fig. S13 Views of a linear (a) and the adjacent parallel linear (b) arrays of discrete $[Pt(dto)]^{2-}$ complex anions of **6** together with the atom numbering [symmetry code: (i) = 1 + *x*, *y*, *z*; (ii) = 1 – *x*, 1 – *y*, 1 – *z*]. Perspective views of the crystal packing of the $[Pt(dto)]^{2-}$ complex anions and Ph_4As^+ countercations along the crystallographic *a* (c) and *b* (d) axes, showing the segregated arrays of cations and anions in the crystallographic *bc* and *ac* planes, respectively. The weak intermolecular C=O···H–C type interactions are represented by dashed lines.

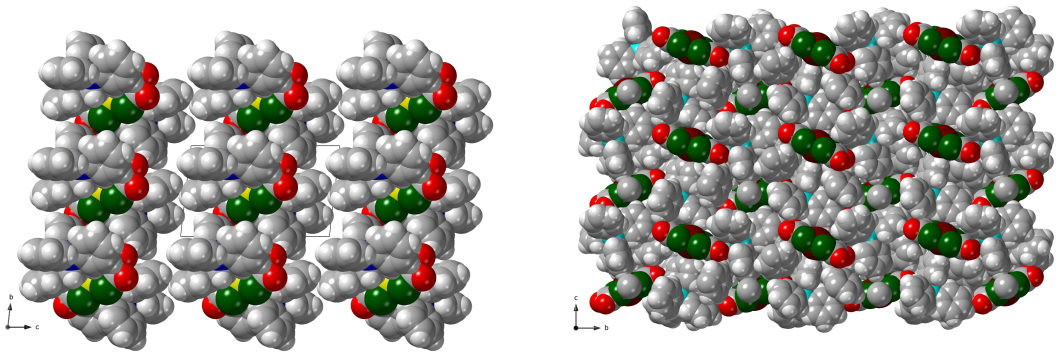

(a) (b)

Fig. S14 Space filling views of **2**·3CH_2Cl_2 (a) and **4**·$(CH_3)_2(CO)$ (b) without the solvent molecules of crystallization showing the differences in terms of the degree of porosity.

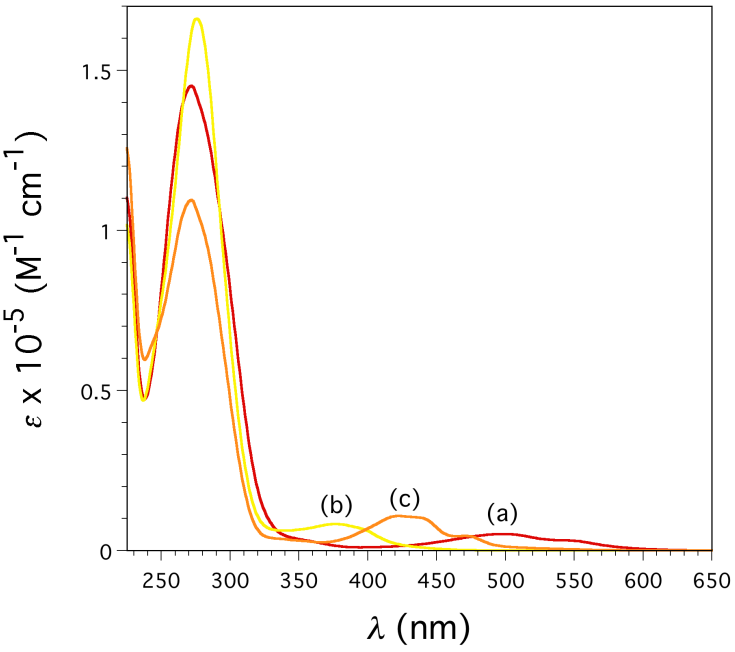

Fig. S15 Electronic absorption spectra of **4** (a), **5** (b) and **6** (c) in acetonitrile at room temperature.

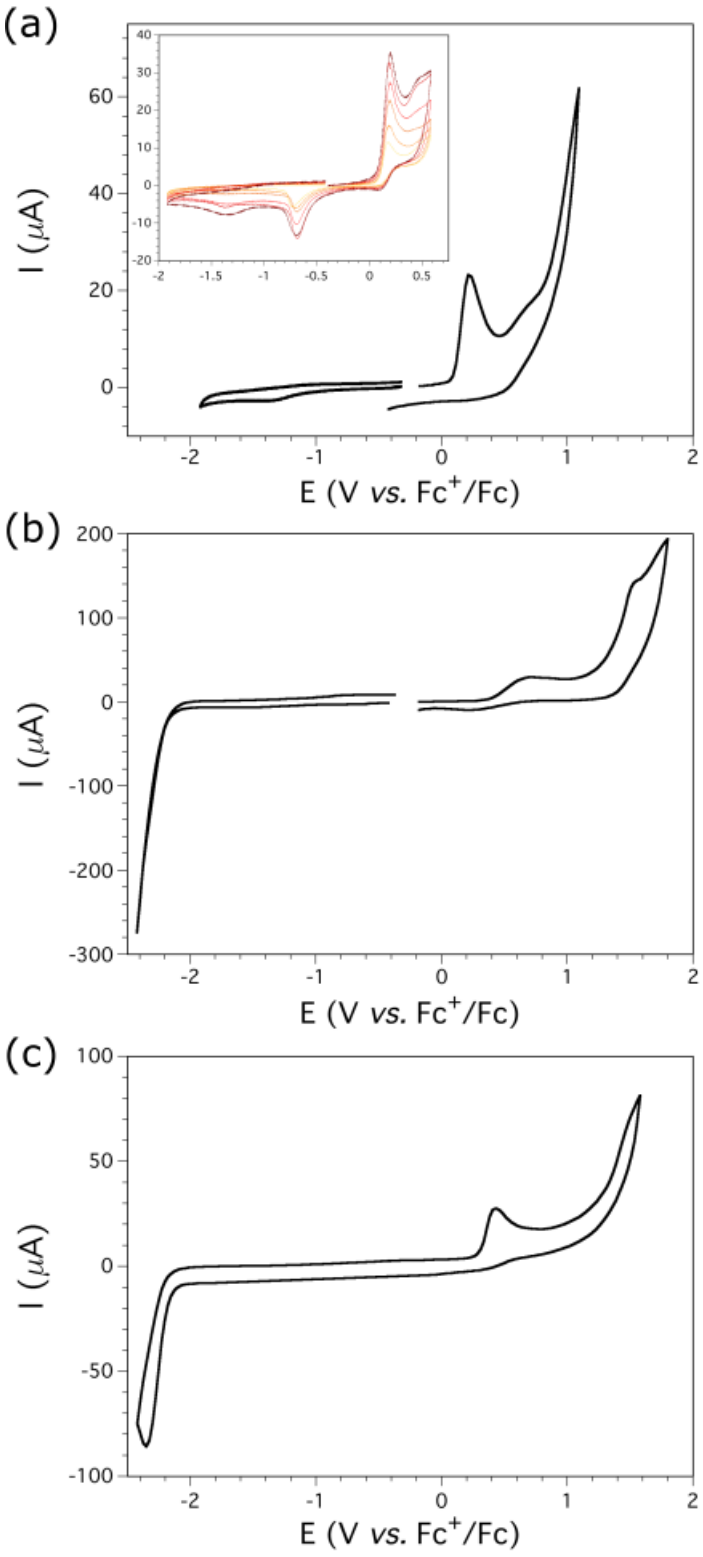

Fig. S16 Cyclic voltammograms of **4** (a), **5** (b) and **6** (c) in acetonitrile at room temperature and at a scan rate of 200 mV s^{-1} (0.1 M *n*-Bu_4NPF_6). The inset shows the cyclic voltammograms for the Ni^{III}/Ni^{II} redox couple of **4** at the scan rate from 25 to 250 mV s^{-1} (yellow to red colors).